



OPEN ACCESS

EDITED BY

Di Wu,
Southwest University, China

REVIEWED BY

Zhongbo Sun,
Changchun University of Technology, China
Jiawang Tan,
Chinese Academy of Sciences (CAS), China
Kaiyuan Yang,
The University of Sheffield, United Kingdom

*CORRESPONDENCE

Jiahao Wu
✉ william_wu.zj@foxmail.com

RECEIVED 17 December 2024

ACCEPTED 08 January 2025

PUBLISHED 05 February 2025

CITATION

Zhao Y, Wu J and Zheng M (2025)
Noise-immune zeroing neural dynamics for
dynamic signal source localization system and
robotic applications in the presence of noise.
Front. Neurobot. 19:1546731.
doi: 10.3389/fnbot.2025.1546731

COPYRIGHT

© 2025 Zhao, Wu and Zheng. This is an
open-access article distributed under the
terms of the [Creative Commons Attribution
License \(CC BY\)](https://creativecommons.org/licenses/by/4.0/). The use, distribution or
reproduction in other forums is permitted,
provided the original author(s) and the
copyright owner(s) are credited and that the
original publication in this journal is cited, in
accordance with accepted academic practice.
No use, distribution or reproduction is
permitted which does not comply with these
terms.

Noise-immune zeroing neural dynamics for dynamic signal source localization system and robotic applications in the presence of noise

Yuxin Zhao¹, Jiahao Wu^{2*} and Mianjie Zheng³

¹School of Humanities, University of Westminster, London, United Kingdom, ²School of Information and Intelligent Engineering, Guangzhou Xinhua University, Guangzhou, Guangdong, China, ³School of Computer Science and Software Engineering, Shenzhen University, Shenzhen, China

Time angle of arrival (AoA) and time difference of arrival (TDOA) are two widely used methods for solving dynamic signal source localization (DSSL) problems, where the position of a moving target is determined by measuring the angle and time difference of the signal's arrival, respectively. In robotic manipulator applications, accurate and real-time joint information is crucial for tasks such as trajectory tracking and visual servoing. However, signal propagation and acquisition are susceptible to noise interference, which poses challenges for real-time systems. To address this issue, a noise-immune zeroing neural dynamics (NIZND) model is proposed. The NIZND model is a brain-inspired algorithm that incorporates an integral term and an activation function into the traditional zeroing neural dynamics (ZND) model, designed to effectively mitigate noise interference during localization tasks. Theoretical analysis confirms that the proposed NIZND model exhibits global convergence and high precision under noisy conditions. Simulation experiments demonstrate the robustness and effectiveness of the NIZND model in comparison to traditional DSSL-solving schemes and in a trajectory tracking scheme for robotic manipulators. The NIZND model offers a promising solution to the challenge of accurate localization in noisy environments, ensuring both high precision and effective noise suppression. The experimental results highlight its superiority in real-time applications where noise interference is prevalent.

KEYWORDS

dynamic signal source localization, robotic manipulator, angle-of-arrival (AoA) scheme, time-difference-of-arrival (TDOA) scheme, trajectory tracking scheme, noise-immune zeroing neural dynamics (NIZND)

1 Introduction

Generally, in a dynamic signal source localization system, a sensor array is deployed within a reasonable range. This array is used to measure real-time dynamic variables, such as time of arrival differences and arrival angles, from a dynamic target object to individual sensors. Subsequently, a mathematical model is established based on the mobile target object's position and the real-time dynamic variables acquired by the sensors. Finally, an appropriate solving method is employed to achieve real-time solutions, obtaining the accurate real-time position of the dynamic signal source.

The solving of dynamic signal source localization (DSSL) problems continues to be utilized in numerous scientific computing and engineering applications. In recent years, an increasing number of scholars have started to work on this class of problems. Such problems play a crucial role in a wide range of applications such as quadrotor positioning (Zhao et al., 2021), robotics (Xie et al., 2024b; Sun et al., 2024), smart furniture (Nassar et al., 2019), mine personnel operations (Zare et al., 2021), and so on (Jin et al., 2024a; Liu et al., 2024, 2022; Wu et al., 2023). However, an overview of real-life production shows that dynamic source location tracking has not been effectively applied in areas where it seems to be urgently needed. For example, in the case of mega-malls (Ali et al., 2019), where satellite coverage is not available but positioning is urgently required, dynamic source location tracking combined with 3D positioning solutions can be used to achieve indoor positioning and thus enable navigation indoors (Guo et al., 2019a; Kunhoth et al., 2020). From a lifestyle perspective, this is much more convenient and practical.

Various source location solutions have proven effective and can be broadly classified into the following three categories. (1) Time of arrival (TOA) scheme, where localization is achieved by measuring the time it takes for a signal emitted from a source to reach several different location sensors. (2) Time of Difference of Arrival (TDOA) scheme, where positioning is achieved by measuring the difference between the time of arrival of the signal from the source at the main sensor and the time of arrival of the signal at each of the other different position sensors, respectively, and then calculating the positioning. (3) Angle of Arrival (AoA) scheme, where positioning is achieved by measuring the angle of arrival of the signal emitted from the source to each of the sensors at different locations (Guo et al., 2019b; Wu et al., 2019a).

The TOA scheme is one of the most common schemes of location. For example, Guo et al. (2019b) proposed a self-clustering measurement combination scheme. The scheme deals with the unclear relationship between the TOA measurement data and signal source in the multi-source location problems. Wu et al. (2019a) introduced synchronization errors into the TOA scheme based on the no-line-of-sight (NLOS) positioning model, which improves the positioning accuracy in NLOS propagation. Besides, to further tolerate measurement errors, NLOS errors, and synchronization errors, Wu et al. (2019b) proposed two new artificial neural network localization schemes and a TOA measurement scheme. As an improvement of the TOA scheme, the TDOA scheme has been the subject of many positioning studies. For instance, Wu P. et al. (2019) proposed a hybrid firefly algorithm (Hybrid FA) scheme that combines the weighted least squares algorithm and FA. This scheme reduces the calculation amount of common passive positioning methods and improves the positioning accuracy (Wu P. et al., 2019). Wang et al. (2020) proposed a TDOA estimation based on Kronecker product decomposition, which applies to effectively identify the relative acoustic impulse response between two microphones. To be suitable for short-distance positioning problems, Pérez-Solano et al. (2020) proposed a UWB indoor positioning system based on the TDOA scheme. To date, various methods have been developed and introduced to improve the AoA scheme. Monfared et al. (2020) used the Non-Data-Aided iterative algorithm to iterate between

angle and position estimation steps to gradually improve the AoA positioning accuracy. Then, Monfared et al. (2021) improved the performance of the AoA scheme by comparing the variance of the middle estimated position of different combinations of all possible anchor point sets with pre-calculated thresholds. In addition, Zhou et al. (2022) proposed an angular domain AoA estimation scheme to locate the user. Another, Hong et al. (2020) studied the AoA positioning in visible light and improved the accuracy of the AoA positioning based on the quadrant-solar-cell and third-order ridge regression machine learning algorithm.

All three of these source localization schemes have their advantages and disadvantages. However, the TOA scheme is simple and has low complexity, but since TOA uses the transmission time of the base station and the target to be measured to calculate the transmission distance to further determine the location of the tag, which requires clock synchronization between each base station and the target to be measured, TOA is susceptible to clock interference in complex indoor environments, resulting in serious errors in positioning accuracy. TDOA scheme, compared with the TOA scheme, does not need to keep the clock synchronization between each base station and the target to be measured, but only needs to synchronize between base stations. This makes the TDOA scheme easier to implement and its application is broader. Compared with the other two schemes, the AoA scheme is suitable for positioning at shorter distances and is generally used as an auxiliary tool for primary coarse positioning (Jin et al., 2016; Ferreira et al., 2005; Jiang and Wang, 2003).

Robotic manipulators have gained significant attention in recent years and have been employed across various fields (Xie et al., 2024a; Jin et al., 2024c; Sun et al., 2003). The trajectory tracking of robotic manipulators is a crucial topic in robotic investigation (Jin et al., 2024b; Xie and Jin, 2023; Lian et al., 2024). In Zhai and Xu (2020), a singularity avoiding sliding mode control was presented, achieving trajectory tracking for robotic manipulators. By leveraging vector pseudo distance, Yang et al. (2022) developed an obstacle avoidance control method for a redundant manipulator, which outperforms traditional methods using Euclidean distance. A learnable motion control strategy was designed in Xu et al. (2020). Through utilizing position and velocity information, it can address the parameter adjusting problem in the controller.

The recurrent neural dynamic (RND) model is often considered a classical intelligent computational approach and has been extensively studied in many scientific and engineering fields (Li et al., 2019a; Zhang et al., 2018; Li et al., 2019b). Neural dynamics transmits and updates information through neurons, representing a brain-inspired algorithm. On this basis, a traditional gradient-based RND model (TGND) was proposed by Xiao et al. (2019) to deal with time-varying matrix inversion problems. However, Jin et al. (2022) pointed out that the TGND model could not make effective use of the time derivative information in solving time-varying problems, and the obtained state solutions would generate a time lag error. As the time lag error can seriously hinder the solution of dynamic localization problems. Therefore, traditional zeroing neural dynamic (TZND) (Dai et al., 2024), named after their inventors, were considered as a way to effectively utilize time derivatives to time-varying problems. Researchers have then continued to explore and investigate and devise various improved

ZND models to solve different time-varying problems, including the application of activation functions. In Yan et al. (2021), A TZND model was proposed to solve a receding horizon control scheme for a redundant manipulator.

On the one hand, as the dimensionality of solving dynamic localization problems and the degrees of freedom of robotic manipulator increases, the currently available methodologies are constructed to have low accuracy and long solution times when dealing with this type of problem. On the other hand, noise interference, as an important factor affecting accuracy, should further enhance the robustness and usability of the existing TZND model to achieve facing various noise disturbances brought about by realistic environments. To this end, a Noise-Immune Zeroing Neural Dynamics (NIZND) model activated by SBP is proposed in this paper to solve the DSSL problem and trajectory tracking scheme under noisy interference conditions. In the ideal environment without noise, the error of this model converges globally to zero; in the conditions of constant and random noise, the proposed NIZND model converges globally to a bounded range. To visually explain the design framework idea of this paper, a graphical representation of structure of this paper is shown in Figure 1.

The remainder of this article is arranged as follows. In Section 2, the DSSL problem is presented and transformed by both TDOA and AoA methods. Next, the specific design procedure of the proposed NIZND model is presented in Section 3, which also presents the derivation of the subsequent simulation part of the comparison models. Then, the corresponding analyses and proofs of the global convergence and robustness of the proposed NIZND model are presented in Section 4. After that, Section 5 provides several sets of illustrative simulation experiments that verify the high accuracy as well as the strong robustness of the NIZND model in its application to TDOA, AoA, and trajectory tracking schemes. Finally, the conclusion is summarized in Section 6.

Before ending the introduction, the main contribution of this paper is listed as follows:

- In this paper, a novel NIZND model is proposed to solve the DSSL and trajectory tracking problem of robotics, which has higher accuracy solution results and faster convergence speed in the iterative process than the traditional ZND model.
- A special activation function termed the SBP function in the real-valued domain is presented for constructing the NIZND model. Furthermore, this paper analyzes the anti-noise performance of the framework under different noise conditions and compares the performance of other models through theorems and proofs.
- Corresponding experimental results are executed for the DSSL problem and robotic problem, and the extraordinary superiority of the NIZND model is demonstrated by designing several sets of controlled simulation experiments.

2 Problem formulation and related work

Generally, the purpose of positioning technology is to set up base stations in a reasonable range, and the actual distance of the target object measured by base stations is calculated by the

scheme to get an accurate target trajectory. In other words, utilizing the coordinates of base stations to measure the distance of the target object (Jin et al., 2020; Dai et al., 2021). Then, we introduce some essential definitions of the positioning schemes to model the geometric relationship between the target object and base stations into a time-varying dynamic matrix system.

2.1 Angle-of-arrival

The AoA scheme via measuring the horizontal and pitch angles between base stations and the target to calculate the intersection point. Then, according to the intersection point of direction line is formed between each base station and the target object to implement the positioning operation. For simplicity, Figure 2 illustrates the principle of the AoA scheme under two base stations. Note that the AoA scheme can be extended to a multi-base stations scheme, which enables to improvement of the performance of this scheme.

Suppose that the horizontal angles and the pitching angles of the m base stations are $\vec{\alpha} = [\alpha_1(t), \dots, \alpha_m(t)]^T \in \mathbb{R}^m$ and $\vec{\beta} = [\beta_1(t), \dots, \beta_m(t)]^T \in \mathbb{R}^m$, respectively. The superscript T indicates the transpose operation of a matrix or vector. The position of the target object at time t is expressed as $\mathbf{p}(t) = [p_x(t), p_y(t), p_z(t)]^T \in \mathbb{R}^3$, and coordinates of base stations are $S = [\vec{s}_1, \vec{s}_2, \dots, \vec{s}_m] \in \mathbb{R}^{3 \times m}$, where $\mathbf{s}_m = [x_m, y_m, z_m] \in \mathbb{R}^3$ (Jin et al., 2020). According to the principle of AoA scheme, the geometric relationship between horizontal and pitch angle is formulated as

$$\alpha_i(t) = \tan\left(\frac{p_y(t) - y_i}{p_x(t) - x_i}\right), \tag{1}$$

$$\beta_i(t) = \tan\left(\frac{p_z(t) - z_i}{\sqrt{(p_x(t) - x_i)^2 + (p_y(t) - y_i)^2}}\right). \tag{2}$$

We further define the dynamic matrix $Q_1(t) \in \mathbb{R}^{2m \times 3}$ and dynamic vector $\vec{h}_1(t) \in \mathbb{R}^{2m}$ as follows:

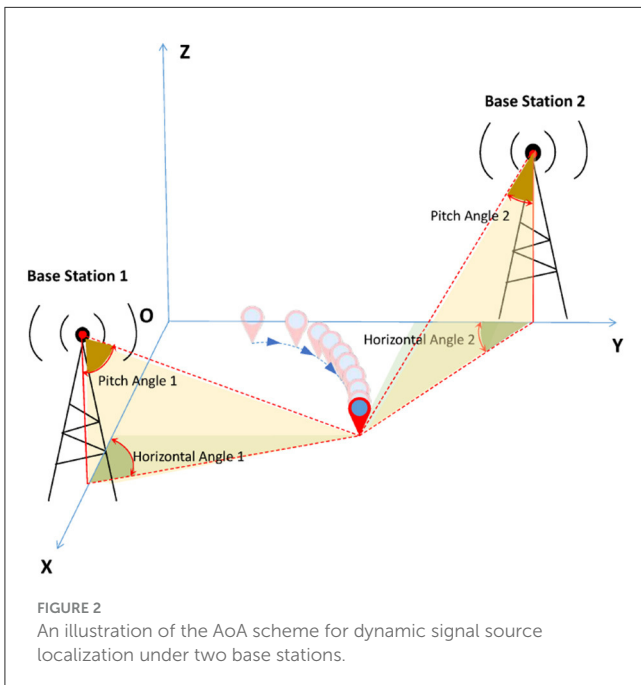
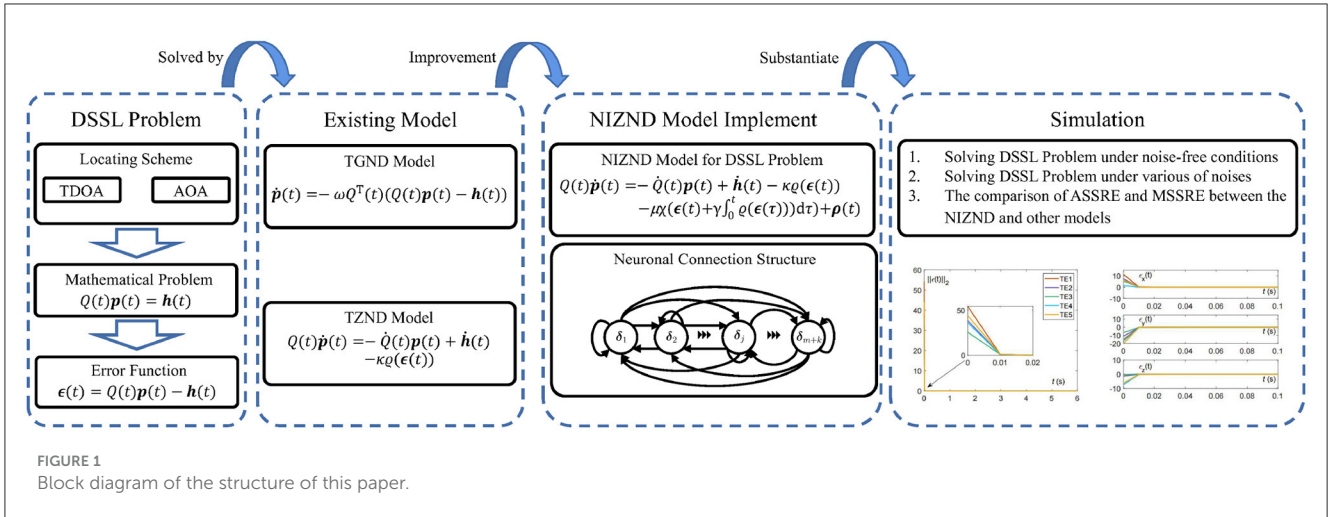
$$Q_1(t) = \begin{bmatrix} \vec{v}_1(t) & \vec{1}_{m \times 1} & \vec{0}_{m \times 1} \\ \vec{0}_{m \times 1} & \vec{v}_2(t) & -\vec{1}_{m \times 1} \end{bmatrix}, \vec{h}_1(t) = \begin{bmatrix} \vec{v}_3(t) \\ \vec{v}_4(t) \end{bmatrix},$$

where vector $\vec{v}_1, \vec{v}_2, \vec{v}_3$, and \vec{v}_4 are constructed as

$$\vec{v}_1(t) = \begin{bmatrix} -\tan \alpha_1(t) \\ \vdots \\ -\tan \alpha_m(t) \end{bmatrix}, \vec{v}_2(t) = \begin{bmatrix} \frac{\tan \beta_1(t)}{\sin \alpha_1(t)} \\ \vdots \\ \frac{\tan \beta_m(t)}{\sin \alpha_m(t)} \end{bmatrix},$$

$$\vec{v}_3(t) = \begin{bmatrix} y_1 - x_1 \tan(\alpha_1(t)) \\ \vdots \\ y_m - x_m \tan(\alpha_m(t)) \end{bmatrix},$$

$$\vec{v}_4(t) = \begin{bmatrix} \frac{y_1 \tan \beta_1(t)}{\sin \alpha_1(t)} - z_1 \\ \vdots \\ \frac{y_m \tan \beta_m(t)}{\sin \alpha_m(t)} - z_m \end{bmatrix}.$$



Therefore, the geometric relationship between the target object $\vec{p}(t)$ and base stations S is constructed as

$$Q_1(t)p(t) = h_1(t). \tag{3}$$

2.2 Time-difference-of-arrival

TDOA is a time difference based localization scheme. The position of a target object is determined by measuring the difference in signal propagation time from the target object to multiple base stations and obtaining its distance difference (Dai et al., 2021).

Firstly, the purpose of TDOA is to utilize time differences to get dynamic distance differences between the target object and the base

station. Such as distance differences:

$$\Delta l_j(t) = l_j(t) - l_1(t) = c\Delta g_j = c(g_j - g_1), \tag{4}$$

where $j \in \{2, \dots, n\}$, symbol c represents the signal transmission speed. Δg_j is the time difference between the arrival of the signal at the j th base station and the first base station. g_j is the time it takes for the signal from the target object to reach the j th base station. $l_j(t)$ denotes the dynamic distance between the target object and j th base station, and it satisfies:

$$\begin{aligned} l_j^2(t) &= (x_j - p_x(t))^2 + (y_j - p_y(t))^2 + (z_j - p_z(t))^2 \\ &= c_j - 2(x_j p_x(t) + y_j p_y(t) + z_j p_z(t)) + p_x^2(t) + p_y^2(t) + p_z^2(t), \end{aligned} \tag{5}$$

where $c_j = x_j^2 + y_j^2 + z_j^2$. Subsequently, combining the Equations 4, 5, we get:

$$\Delta l_j^2(t) + 2l_1(t)\Delta l_j(t) = c_j - c_1 - 2(\Delta x p_x(t) + \Delta y p_y(t) + \Delta z p_z(t)),$$

where $\Delta x = x_j - x_1$, $\Delta y = y_j - y_1$, $\Delta z = z_j - z_1$. The following matrix Q_2 and dynamic vector $\vec{h}_2(t)$ are furnished for further implementing the TDOA scheme (Equation 4):

$$Q_2 = \begin{bmatrix} x_{21} & y_{21} & z_{21} \\ x_{31} & y_{31} & z_{31} \\ \vdots & \vdots & \vdots \\ x_{n1} & y_{n1} & z_{n1} \end{bmatrix} \in \mathbb{R}^{n \times 3},$$

$$\vec{h}_2(t) = \begin{bmatrix} \frac{1}{2}(c_2 - c_1 - \Delta l_2^2(t)) - \Delta l_2(t)l_1(t) \\ \frac{1}{2}(c_3 - c_1 - \Delta l_3^2(t)) - \Delta l_3(t)l_1(t) \\ \vdots \\ \frac{1}{2}(c_n - c_1 - \Delta l_n^2(t)) - \Delta l_n(t)l_1(t) \end{bmatrix} \in \mathbb{R}^n.$$

Now, the TDOA scheme (Equation 4) is converted into the following as $Q_2(t)p(t) = h_2(t)$. In summary, the AoA (Equations 1, 2) and TDOA scheme (Equation 4) based DSSL can be transformed as the following dynamic linear equation problem:

$$Q(t)p(t) = h(t). \tag{6}$$

3 NIZND model formulate

In this section, we construct the NIZND model to realize the AoA (Equations 1, 2) and TDOA scheme (Equation 4). To solve the DSSL problem (Equation 6) effectively, we first present the design process of the TGND model and the TZND model. Then, the second part designs the NIZND model with noise immunity based on the existing models.

3.1 Existing problem solver

The TGND model based on the gradient descent idea is often used to solve dynamic matrix system optimization problems (Tang and Zhang, 2023; Zhang et al., 2024; Lv et al., 2019). To monitor the performance of the model at any time, a performance metric called the error function is designed as

$$\epsilon(t) = Q(t)p(t) - h(t) \in \mathbb{R}^n. \tag{7}$$

Then, a squared operation based on the error function can be written as $e(t) = \|\epsilon(t)\|_2^2/2$. Moreover, according to the design philosophy of the TGND model (Xiao et al., 2020), we have:

$$-\frac{\partial e(t)}{\partial p(t)} = -Q^T(t)\epsilon(t). \tag{8}$$

Finally, according to the above negative gradient descent information, one has:

$$\begin{aligned} \dot{p}(t) &= -\omega Q^T(t)\epsilon(t) \\ &= -\omega Q^T(t)(Q(t)p(t) - h(t)), \end{aligned} \tag{9}$$

where the parameter $\omega > 0$ represents a scalar-valued factor used to control the convergence rate of TGND model (Equation 9).

As well as the TGND model (Equation 9), the TZND model is also a widely applied (Liao et al., 2024, 2022; Sun et al., 2022) and effective method for solving time-varying linear matrix systems (Equation 6). To begin with, the error function setting rules are the same as in equation (Equation 7). Then, the corresponding TZND model can be derived from the design formula:

$$\dot{\epsilon}(t) = -\kappa \varrho(\epsilon(t)), \tag{10}$$

where $\kappa > 0$ denotes a fixed parameter designed to control the speed of the solution process, and $\varrho(\cdot)$ denotes the scalar-oriented activation function. From the above equation, the following equation can be formulated as follow:

$$Q(t)\dot{p}(t) = -\dot{Q}(t)p(t) + \dot{h}(t) - \kappa \varrho(\epsilon(t)). \tag{11}$$

3.2 NIZND model construction

The evolution function of the proposed NIZND model is formulated as

$$\dot{\epsilon}(t) = -\gamma \varrho(\epsilon(t)) - \mu \chi \left(\epsilon(t) + \gamma \int_0^t \varrho(\epsilon(\tau))d\tau \right), \tag{12}$$

where $\gamma > 0 \in \mathbb{R}$ and $\mu > 0 \in \mathbb{R}$ are the design parameters. Symbol $\chi(\cdot)$ denotes the feedback-oriented activation function. In this paper, the following three activation functions are used to activate the model:

3.2.1 Simplified activation function

$$\varrho(\epsilon_i) = k * \text{Lip}^\iota(\epsilon_i).$$

3.2.2 Sign-bi-power function

$$\varrho(\epsilon_i) = a_1 * \text{Lip}^\iota(\epsilon_i) + a_2 * \text{Lip}^{\frac{1}{\iota}}(\epsilon_i).$$

3.2.3 Combined activation function

$$\varrho(\epsilon_i) = b_1 \text{Lip}^\iota(\epsilon_i) + b_2 \epsilon_i.$$

Futhermore, the function $\text{Lip}^\iota(\cdot)$ can be defined as

$$\text{Lip}^\iota(\epsilon_i) = \begin{cases} |\epsilon_i|^\iota, & \epsilon_i > 0, \\ 0, & \epsilon_i = 0, \\ -|\epsilon_i|^\iota, & \epsilon_i < 0, \end{cases}$$

where $\iota > 0$. Consequently, it can be concluded that the proposed NIZND model with adaptive activation function for solving the DSSL problem (Equation 6) is written as

$$\begin{aligned} Q(t)\dot{p}(t) &= -\dot{Q}(t)p(t) + \dot{h}(t) - \gamma \varrho(\epsilon(t)) \\ &\quad - \mu \chi \left(\epsilon(t) + \gamma \int_0^t \varrho(\epsilon(\tau))d\tau \right). \end{aligned} \tag{13}$$

Allowing for different noises interference, in order to further analyze and verify the influence of various noises on the NIZND model (Equation 13), the following form of the NIZND model (Equation 13) disordered by measurement noises is deemed:

$$\begin{aligned} Q(t)\dot{p}(t) &= -\dot{Q}(t)p(t) + \dot{h}(t) - \gamma \varrho(\epsilon(t)) \\ &\quad - \mu \chi \left(\epsilon(t) + \gamma \int_0^t \varrho(\epsilon(\tau))d\tau \right) + \rho(t), \end{aligned} \tag{14}$$

where $\rho(t) \in \mathbb{R}^n$ is the inevitable noise during positioning. The system update is performed by $p(t)$ acting as neurons, and the proposed NIZND is a brain-inspired algorithm.

4 The theoretical analysis

In this section, the convergence of the NIZND model (Equation 13) to solve the DSSL problem (Equation 6) under ideal conditions and its robustness to different localization noises are demonstrated through theoretical analysis. Four theorems and corresponding proof procedures are summarized below.

4.1 Convergence

Theorem 1: Considering the DSSL problem (Equation 6) with non-noise perturbed, starting from any initial position within a certain range, the positional states generated by the proposed NIZND model (Equation 13) will converge to the theoretical position of the DSSL problem (Equation 6). That is to say, the residual error $\|\epsilon(t)\|_2$ produced by the NIZND model (Equation 13) globally converges to zero.

Proof: First, a Lyapunov function is constructed for analyzing the convergence performance of the NIZND model (Equation 13):

$$F_1(t) = \frac{\epsilon^T(t)\epsilon(t)}{2} \begin{cases} > 0, & \epsilon(t) \neq 0, \\ = 0, & \epsilon(t) = 0. \end{cases} \quad (15)$$

Taking into account the subsequent proof process, let us define

$$\zeta(t) = \epsilon(t) + \int_0^t \varrho(\epsilon(\tau))d\tau. \quad (16)$$

Thus, the derivative of $\zeta(t)$ with respect to t can be written as

$$\dot{\zeta}(t) = \frac{d\zeta(t)}{dt} = \dot{\epsilon}(t) + \varrho(\epsilon(t)). \quad (17)$$

Without loss of generality, the fixed parameters in the NIZND model (Equation 13) are set as $\gamma = \mu = 1$. Then, substituting Equation 13 into Equation 18, we can obtain:

$$\dot{\zeta}(t) = -\Psi(\epsilon(t)). \quad (18)$$

In the same principle as the construction of Equation 15, another Lyapunov equation is defined as

$$F_2(t) = \frac{\zeta^T(t)\zeta(t)}{2} \begin{cases} > 0, & \zeta(t) \neq 0, \\ = 0, & \zeta(t) = 0. \end{cases} \quad (19)$$

Consequently, the derivative of the Equation 19 is:

$$\dot{F}_2(t) = -\zeta^T(t)\varrho(\epsilon(t)) \begin{cases} < 0, & \zeta(t) \neq 0, \\ = 0, & \zeta(t) = 0. \end{cases} \quad (20)$$

Since $F_2(t)$ is positive definite when $\zeta(t) \neq 0$ and $\dot{F}_2(t)$ is negative definite when $\zeta(t) \neq 0$. Therefore, according to Lyapunov stability analysis, $\zeta(t)$ globally converges to zero. Furthermore, when $\zeta(t) = 0$, it follows from the LaSalle's invariance principle that (Equation 18) can be reformulated as

$$\dot{\epsilon}(t) = -\varrho(\epsilon(t)). \quad (21)$$

In light of the Equation 21, the time derivative of Equation 15 is expressed as

$$\dot{F}_1(t) = -\epsilon^T(t)\varrho(\epsilon(t)) \begin{cases} < 0, & \epsilon(t) \neq 0, \\ = 0, & \epsilon(t) = 0. \end{cases} \quad (22)$$

Similarly, Equations 15, 22 satisfy Lyapunov's second theorem, the error function $\epsilon(t)$ can converge to zero globally. The proof is completed.

4.2 Robustness

Theorem 2: The residual error $\|\epsilon(t)\|_2$ of the constant noise $\rho(t) = \rho \in \mathbb{R}^n$ perturbed NIZND model (Equation 13) for solving the DSSL (Equation 6) globally converges to zero in the situation of $-\mu\chi(\zeta(t)) + \rho \leq 0$. The parameter $\zeta(t)$ represents the intermediate variable which is definition as Equation 16.

Proof: For the convenience of further derivation and analysis, the time derivative of intermediate variable $\zeta(t)$ with constant noise ρ is written as $\dot{\zeta}(t) = -\mu\chi(\zeta(t)) + \rho$, and its i th subelement is:

$$\dot{\zeta}_i(t) = -\mu\chi(\zeta_i(t)) + \rho_i. \quad (23)$$

We present the following Lyapunov candidate function $F_3(t) = \zeta_i^2(t)/2$ and its time derivative is written as

$$\dot{F}_3(t) = \zeta_i(t) (-\mu\chi(\zeta_i(t)) + \rho_i). \quad (24)$$

Obviously, the sign of the $\zeta_i(t)$ will affect the positive and negative of $\dot{F}_3(t)$. Therefore, we divide $\zeta_i(t)$ into three situations and discussed them in detail one by one.

4.2.1 $\zeta_i(t) < 0$

In this case, according to the definition of power bounded adaptive function, we have $\chi(\zeta_i(t)) < 0$. Consequently, the following three subcases are provided to guarantee the negative definiteness of $\dot{F}_3(t)$.

- Firstly, in the situation of $-\mu\chi(\zeta_i(t)) + \rho_i > 0$. On account of $\zeta_i(t) < 0$ and Equation 24, the time derivative of candidate function $\dot{F}_3(t) < 0$. Therefore, according to the Lyapunov theory, we can summarize that the system (Equation 23) is globally convergent. That is to say, $-\mu\chi(\zeta_i(t))$ approaches to constant noise ρ_i over time until $-\mu\chi(\zeta_i(t)) + \rho_i = 0$. In addition, the convergence performance of model (Equation 23) will be demonstrated in the following text simulation.
- Secondly, in the situation of $-\mu\chi(\zeta_i(t)) + \rho_i = 0$. Evidently, it can infer that $\dot{F}_3(t) = 0$ and $\zeta_i(t) = \chi^{-1}(\rho_i/\mu)$. In general, the system (Equation 23) is steady and $\zeta_i(t)$ convergent to a ball surface will be verified again by the following simulation.
- Thirdly, in the situation of $-\mu\chi(\zeta_i(t)) + \rho_i < 0$. Due to $\zeta_i(t) < 0$ and $-\mu\chi(\zeta_i(t)) + \rho_i < 0$, $\dot{F}_3 > 0$. It can be readily deduced that the system (Equation 23) diverges and the absolute value of $\chi(\zeta_i(t))$ grows bigger due to the absolute value of $\zeta_i(t)$ turn larger. In light of the power-bounded adaptive activation function's upper $\chi+$ and lower $\chi-$ bounds will influence the robustness of the system (Equation 23) in this situation, therefore, we further divide the situation into the following two subcases. When $\mu\chi- \leq \rho_i$, there always exists a time instant t to transform system (Equation 23) in to case of $-\mu\chi(\zeta_i(t)) + \rho_i = 0$, which infer the system tend to steady. On the contrary, when $\mu\chi- > \rho_i$, the system (Equation 23) diverges as time evolves. Consequently, to avoid the divergence of the system, it is necessary to properly adjust the value of scale parameter μ in Equation 23 as well as Equation 13.

4.2.2 $\zeta_i(t) = 0$

Obviously, in this sense $\chi(\zeta_i(t)) = 0$ and $\dot{\zeta}_i(t) = \rho_i$. It manifests that $\zeta_i(t) > 0$ when constant noise $\rho_i > 0$ or $\zeta_i(t) < 0$ when $\rho_i < 0$. Accordingly, $\zeta_i(t)$ only exist as a transient state and the system (Equation 23) is unstable when $\rho_i \neq 0$, which indicates the situation will turn back to case in $\zeta_i(t) < 0$ or $\zeta_i(t) > 0$.

4.2.3 $\zeta_i(t) > 0$

The situation in this part is similar to the situation when $\zeta_i(t) < 0$, so it is omitted there.

In view of $0 < \rho < \mu\chi +$ or $\mu\chi - < \rho < 0$, $\lim_{t \rightarrow \infty} \zeta(t) = \chi^{-1}(\rho/\mu)$. Next, it can be obtained that $\lim_{t \rightarrow \infty} \dot{\zeta}(t) = 0$. Thus, according to the above conditions, at time t tending to infinity, $\dot{\zeta}(t) = \dot{\epsilon}(t) + \gamma\varrho(\epsilon(t)) = 0$. The following equation is derived from Equation 12:

$$\dot{\epsilon}(t) = -\gamma\varrho(\epsilon(t)). \tag{25}$$

The derivation of Equation 25 can be obtained from Theorem 1, so the proof is omitted here. Further, in view of $0 < \rho < \mu\chi +$ or $\mu\chi - < \rho < 0$, $\dot{\zeta}(t) = -\mu\chi(\zeta(t)) + \rho \leq 0$, that is to say, the NIZND model (Equation 13) for solving the DSSL (Equation 6) globally converges to zero.

The proof is completed.

Theorem 3: Beginning with a randomly generated initial position vector $p(0)$, the residual error of the NIZND (Equation 13) model perturbed by the bounded random noise $\tilde{h}(t)$ converges to a bounded range, where $\rho(t) = \tilde{h}(t) \in \mathbb{R}^n$ represents the bounded random noise.

Proof: Taking into account the interference of bounded random noise $\tilde{h}(t)$, the activation function is set uniformly as a linear activation function, so that the NIZND model (Equation 13) be equivalent to the following equation in this situation as follows:

$$\dot{\epsilon}(t) = (-\gamma - \mu)\epsilon(t) - \gamma\mu \int_0^t \epsilon(\tau) d\tau. \tag{26}$$

By defining

$$s_i(t) = \begin{bmatrix} \epsilon_i(t) \\ \int_0^t \epsilon_i(\tau) d\tau \end{bmatrix}, V = \begin{bmatrix} -\gamma - \mu & -\gamma\mu \\ 1 & 0 \end{bmatrix}, w = \begin{bmatrix} 1 \\ 0 \end{bmatrix},$$

the Equation 26 can be written as

$$\dot{s}_i = Vs_i(t) + wh_i(t), \tag{27}$$

where $\tilde{h}_i(t)$ denoted the i th element of the bounded random noise $\tilde{h}(t)$. Moreover, it is elicited that:

$$s_i(t) = \exp(Vt)s_i(0) + \int_0^t \exp(V(t-\tau))wh_i(\tau) d\tau. \tag{28}$$

In terms of the definition of the triangle inequality, the following inequation is obtained as

$$\begin{aligned} \|s_i(t)\|_2 &\leq \|\exp(Vt)s_i(0)\|_2 \\ &\quad + \left\| \int_0^t \exp(V(t-\tau))wh_i(\tau) d\tau \right\|_2 \\ &\leq \|\exp(Vt)s_i(0)\|_2 \\ &\quad + \int_0^t \|\exp(V(t-\tau))w\|_2 |\tilde{h}_i(\tau)| d\tau. \end{aligned} \tag{29}$$

To further solve the linear differential equation with higher order constant coefficients (Equation 26), it can be divided into the following three cases according to the parameter $\Delta = (\gamma + \mu)^2 - 4\gamma\mu$.

Case I: For the case of $\Delta > 0$, it can be easily premised that $\Gamma_{1,2} = ((-\gamma - \mu) \pm \sqrt{(\gamma + \mu)^2 - 4\gamma\mu}) / 2$, from which $\Gamma_1 \neq \Gamma_2$. Thus, it can be gotten that:

$$\exp(Vt)s_i(0) = \begin{bmatrix} \frac{\epsilon_i(0)(\Gamma_1 \exp(\Gamma_1 t) - \Gamma_2 \exp(\Gamma_2 t))}{\Gamma_1 - \Gamma_2} \\ \frac{\epsilon_i(0)(\exp(\Gamma_1 t) - \exp(\Gamma_2 t))}{\Gamma_1 - \Gamma_2} \end{bmatrix},$$

$$\exp(Vt)w = \begin{bmatrix} \frac{(\Gamma_1 \exp(\Gamma_1 t) - \Gamma_2 \exp(\Gamma_2 t))}{\Gamma_1 - \Gamma_2} \\ \frac{(\exp(\Gamma_1 t) - \exp(\Gamma_2 t))}{\Gamma_1 - \Gamma_2} \end{bmatrix},$$

where $\Gamma_1 = -\mu$, $\Gamma_2 = -\gamma$, $\Gamma_1 \neq \Gamma_2$. In order to discuss the magnitude of the values of A and B, they are divided into two cases for analysis in detail.

- For the subcase of $\Gamma_1 > \Gamma_2$, it is naturally acquired that $(\Gamma_1 \exp(\Gamma_1 t) - \Gamma_2 \exp(\Gamma_2 t)) / (\Gamma_1 - \Gamma_2) < \exp(\Gamma_1 t)$ and $(\exp(\Gamma_1 t) - \exp(\Gamma_2 t)) / (\Gamma_1 - \Gamma_2) < \exp(\Gamma_1 t) / (\Gamma_1 - \Gamma_2)$. Thus, it is further obtained that:

$$\|\exp(Vt)s_i(t)\|_2 \leq \frac{\sqrt{(\gamma - \mu)^2 + 1}}{\gamma - \mu} \exp(\Gamma_1 t) |\epsilon_i(0)|,$$

$$\|\exp(Vt)w\|_2 \leq \frac{\sqrt{(\gamma - \mu)^2 + 1}}{\gamma - \mu} \exp(\Gamma_1 t).$$

Then, we could get:

$$\begin{aligned} |\epsilon_i(t)| \leq \|s_i(t)\|_2 &\leq \frac{\sqrt{(\gamma - \mu)^2 + 1}}{\gamma - \mu} \exp(\Gamma_1 t) |\epsilon_i(0)| \\ &\quad - \frac{\sqrt{(\gamma - \mu)^2 + 1}}{\Gamma_1(\gamma - \mu)} \max_{0 < \tau < t} |\tilde{h}_i(\tau)|. \end{aligned}$$

At last, the upper bound of error can be calculated as follows:

$$\limsup_{t \rightarrow \infty} \|\epsilon(t)\|_2 \leq \frac{\psi \sqrt{k((\gamma - \mu)^2 + 1)}}{\mu(\gamma - \mu)}.$$

- For the subcase of $\Gamma_1 < \Gamma_2$, likewise, the proof process is the same as for $\Gamma_1 > \Gamma_2$. Thus, we can deduce that $\lim_{t \rightarrow \infty} \sup \|\epsilon(t)\|_2 \leq \frac{\psi \sqrt{k((\gamma - \mu)^2 + 1)}}{\mu(\gamma - \mu)}$. **Case II:** For the case of $\Delta = 0$, it can be clearly inferred that $\mu = \gamma$. In view of the above condition, we can know that:

$$\exp(Vt)s_i(0) = \begin{bmatrix} \epsilon_i(0)\Gamma_1 t \exp(\Gamma_1 t) \\ \epsilon_i(0)t \exp(\Gamma_1 t) \end{bmatrix},$$

$$\exp(Vt)w = \begin{bmatrix} \Gamma_1 t \exp(\Gamma_1 t) \\ t \exp(\Gamma_1 t) \end{bmatrix},$$

from which $\Gamma_1 = \Gamma_2 = \frac{-\gamma - \mu}{2}$. According to the proof of Lemma 1 in , $t\sqrt{\Gamma_1^2 + 1} \exp(\Gamma_1 t) < \nu \exp(-\delta t)$ with $\nu > 0, \delta > 0$.

$$\|\exp(Vt)\mathbf{w}\|_2 = t\sqrt{\Gamma_1^2 + 1} \exp(\Gamma_1 t) < \nu \exp(-\delta t),$$

and

$$|\epsilon_i(t)| \leq \|\mathbf{s}_i(t)\|_2 \leq \nu \exp(-\delta t) |\epsilon_i(0)| + \frac{\nu}{\delta} \max_{0 < \tau < t} |h_i(\tau)|.$$

Finally,

$$\limsup_{t \rightarrow \infty} \|\epsilon(t)\|_2 \leq \frac{\psi \nu \sqrt{k}}{\delta},$$

where $\psi = \max_{1 \leq i \leq k} \{\max_{0 \leq \tau \leq t} |h_i(\tau)|\}$. Therefore, perturbed by the bounded random noise $\mathbf{h}(t)$, the residual errors $\epsilon(t)$ of the proposed NIZND model (Equation 13) for solving DSSL problem (Equation 6) are bounded. The proof is completed.

5 Illustrative simulation experiments

In this section, corresponding localization examples and compare experiments are designed and performed to demonstrate the feasibility, efficiency, and superiority of the proposed NIZND model (Equation 13). Note that all the following simulation experiments are run on a computer with an AMD Ryzen 5 5600H with Radeon Graphics @3.30 GHz CPU, 16-GB memory, NVIDIA GeForce RTX 3050 GPU, and Windows 11, 64-bit operating system.

5.1 Simulation experiments on AoA

Firstly, five sets of randomly-generated initial states are utilized to solve the DSSL problem (Equation 6) by using the NIZND model (Equation 13), with the corresponding initial conditions picked as follows. We choose the number of base stations to be 8, the coordinates of base stations:

$$S = \begin{bmatrix} -11 & 10 & -11 & 10 & -11 & 10 & -11 & 10 \\ -10 & -10 & 10 & 10 & -10 & -10 & 10 & 10 \\ -10 & -10 & -10 & -10 & 30 & 30 & 30 & 30 \end{bmatrix},$$

the five sets of randomly-generated initial states:

$$P(0) = \begin{bmatrix} -5 & -2 & 0.5 & -2 & -5 \\ 5 & 3 & 2.5 & -3 & 0 \\ 0 & -5 & -0.5 & -2 & -5 \end{bmatrix},$$

the trajectory position of the target object in 3-D space:

$$\mathbf{p}^*(t) = \begin{bmatrix} 5\cos(5t) \\ 5\sin(5t) \\ 10t \end{bmatrix},$$

the scalar-oriented and the feedback-oriented activation function:

$$\varrho(\epsilon_i) = 20 * \text{Lip}^3(\epsilon_i) + 20 * \text{Lip}^{\frac{1}{3}}(\epsilon_i).$$

Secondly, the purpose of Figure 3 is to demonstrate the validity of Theorem 1 by means of the AoA scheme (Equations 1, 2). Specifically, the simulation results among the five sets of initial values solved by the proposed NIZND model (Equation 13) of AoA scheme (Equations 1, 2) are demonstrated in Figure 3. As shown in Figures 3A–D, a comparison of five different initial values of results reveals that the trajectories of the five sets of random initial values approximately coincide with the theoretical value trajectory. Moreover, it is worth noting that from Figures 3E–G, the performance is evaluated from the linear representation, logarithmic representation of approximation errors, and the components of approximation errors in the x,y,z directions, which prove that the proposed NIZND model (Equation 13) globally converges to zero. Therefore, the proposed NIZND model (Equation 13) can be solved for the DSSL problem (Equation 6) at a certain time by the AoA scheme (Equations 1, 2). Similarly, the results of the correlational analysis are set out in Table 1. The average steady-state residual error and maximum steady-state residual error of the NIZND model (Equation 13) converge to 2.918×10^{-3} and 6.402×10^{-3} when $\gamma = \mu = 3$, 8.627×10^{-3} and 1.885×10^{-3} when $\gamma = \mu = 20$, which is less than the two residual errors of TGND model (Equation 9) and TZND model (Equation 11) under the same conditions.

5.2 Simulation experiments on TDOA

In this part, the experiments on the TDOA scheme 4 shown in Figure 4 also reveal the validity of Theorem 1. For comparison, initial conditions for the TDOA scheme 4 simulation experiments are the same as in the previous section. The corresponding performance comparisons of the proposed NIZND model (Equation 13) are referenced by Figure 4 and Table 2. From the overlap degree in Figures 4A–D, choosing five sets of random initial values, the NIZND model (Equation 13) can gradually converge to a theoretical solution by solving the DSSL problem (Equation 6) with the TDOA scheme (Equation 4) in a noise-free operating environment. Additionally, the results obtained from the preliminary analysis of convergence performance can be seen that the proposed NIZND model (Equation 13) globally converges to zero in Figures 4E–G. Overall, the TDOA scheme (Equation 4) can be solved by the proposed NIZND model (Equation 13) and used to solve the DSSL problem (Equation 6). Further analysis of the data is presented in Table 2. As can be seen from the table above, the first group reported significantly less average steady-state residual error and maximum steady-state residual error than the other three groups under the same model. Moreover, the average steady-state residual error and maximum steady-state residual error for the NIZND model (Equation 13) are 3.917×10^{-5} and 7.236×10^{-5} , respectively, when the coefficients $\gamma = \mu = 3$; and 3.895×10^{-4} and 7.207×10^{-4} , respectively, when the coefficients $\gamma = \mu = 20$. Taken together, these results show that the convergence accuracy of the proposed NIZND model (Equation 13) for solving the DSSL

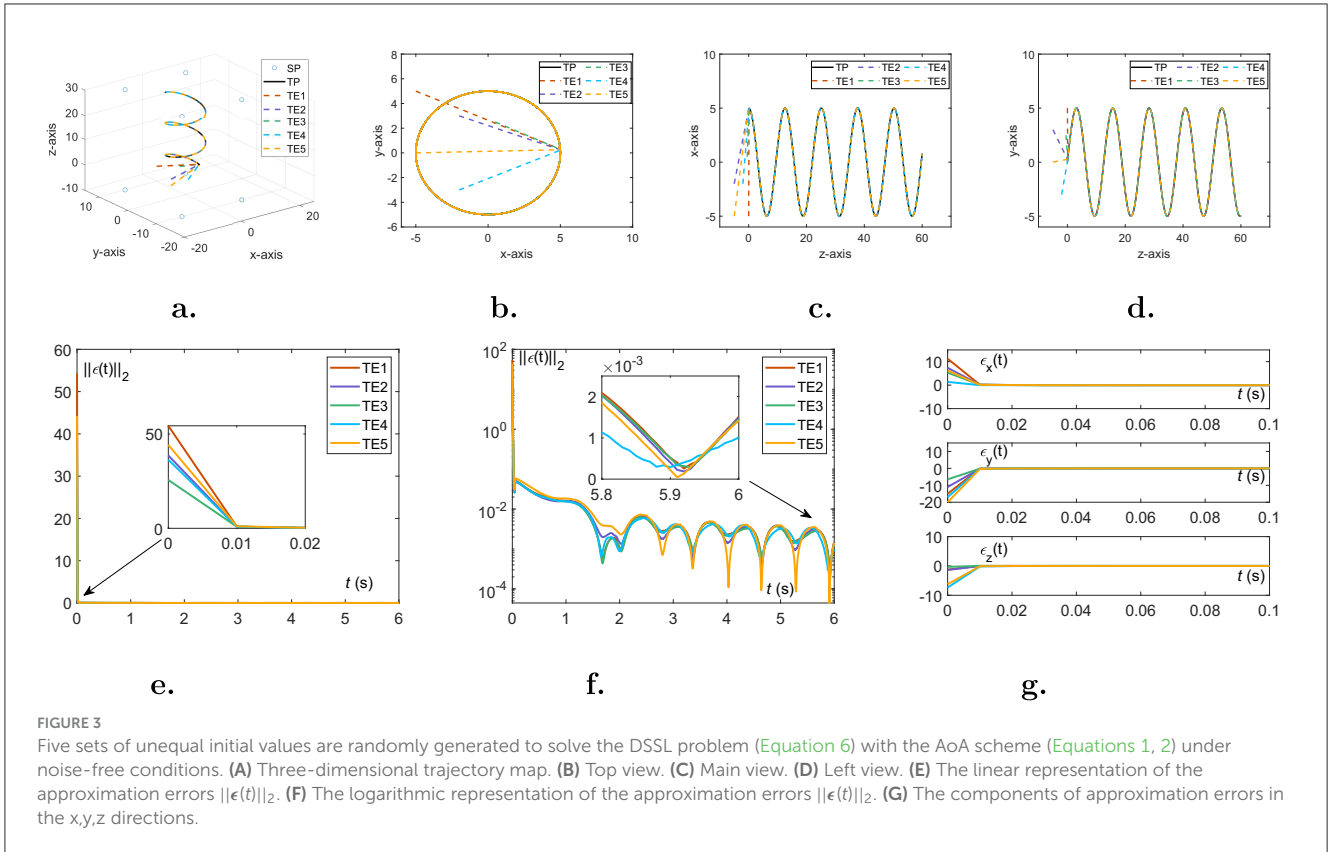


FIGURE 3

Five sets of unequal initial values are randomly generated to solve the DSSL problem (Equation 6) with the AoA scheme (Equations 1, 2) under noise-free conditions. (A) Three-dimensional trajectory map. (B) Top view. (C) Main view. (D) Left view. (E) The linear representation of the approximation errors $\|\epsilon(t)\|_2$. (F) The logarithmic representation of the approximation errors $\|\epsilon(t)\|_2$. (G) The components of approximation errors in the x,y,z directions.

TABLE 1 Comparison of the average steady-state residual error (ASSRE) and maximum steady-state residual error (MSSRE) among TGND model, TZND model, and the proposed NIZND model (Equation 13) when solving the DSSL problem (Equation 6) using the AoA scheme (Equations 1, 2).

Model	Parameters	Average steady-state residual error				Maximal steady-state residual error			
		with NF*	with CN*	with LN*	with RN*	with NF*	with CN*	with LN*	with RN*
TGND	$\omega = 3$	2.325×10^0	2.252×10^1	Infinity	1.084×10^1	3.010×10^0	2.520×10^1	Infinity	1.208×10^1
	$\omega = 20$	3.385×10^{-1}	2.347×10^1	Infinity	1.166×10^1	4.614×10^{-1}	2.467×10^1	Infinity	1.248×10^1
TZND	$\kappa = 3$	1.784×10^{-2}	7.879×10^0	Infinity	3.959×10^0	7.809×10^{-2}	8.654×10^0	Infinity	4.179×10^0
	$\kappa = 20$	7.401×10^{-3}	1.181×10^0	Infinity	5.926×10^{-1}	2.844×10^{-2}	1.236×10^0	Infinity	7.181×10^{-1}
NIZND	$\gamma = 3, \mu = 3$	2.918×10^{-3}	1.239×10^{-2}	3.352×10^{-2}	1.706×10^{-2}	6.402×10^{-3}	2.422×10^{-2}	3.983×10^{-2}	3.993×10^{-2}
	$\gamma = 20, \mu = 20$	8.267×10^{-4}	1.145×10^{-3}	1.472×10^{-3}	3.267×10^{-3}	1.885×10^{-3}	2.736×10^{-3}	3.116×10^{-3}	8.667×10^{-3}

*NF, CN, LN, and RN indicate noise free, constant noise 8, linear noise 2t, and random noise $8 \times [0, 1]$, respectively.

problem (Equation 6) under the same conditions is higher than that of the other two models.

5.3 Performance under noise perturbed

In this part, the approximation errors of two localization schemes are presented in the form of residual plots and numerical tables to show the experimental results of solving the DSSL problem (Equation 6) under various noisy environments, i.e., constant noise $\rho(t) = 8$, linear noise $\rho(t) = 2t$, and random noise $\rho(t) \in 8 \times [0, 1]$. As a comparison, the experimental results of AoA scheme (Equations 1, 2) and TDOA scheme 4 are generated by three models, i.e., TGND model

(9), TZND model (11), and the proposed NIZND model (13). The corresponding localization results are shown in Figures 5, 6 and Tables 1, 2. Figures 5, 6 demonstrate the approximation errors $\|\epsilon(t)\|_2$ of AoA and TDOA scheme under three kinds of noises with parameters $\omega = \kappa = \gamma = \mu = 3$, respectively.

From the visualization results in Figures 5A, D, it can be seen that the proposed NIZND model (Equation 13) converges promptly to 10^{-2} under constant noises, at which point the proposed NIZND model (13) yields better convergence accuracy than the TGND (Equation 9) and TZND models (Equation 11). At the same time, Figures 5B, E illustrates the proposed NIZND model (Equation 13) converges smoothly to 10^{-2} under the linear noise, while those of the TGND (Equation 9) and

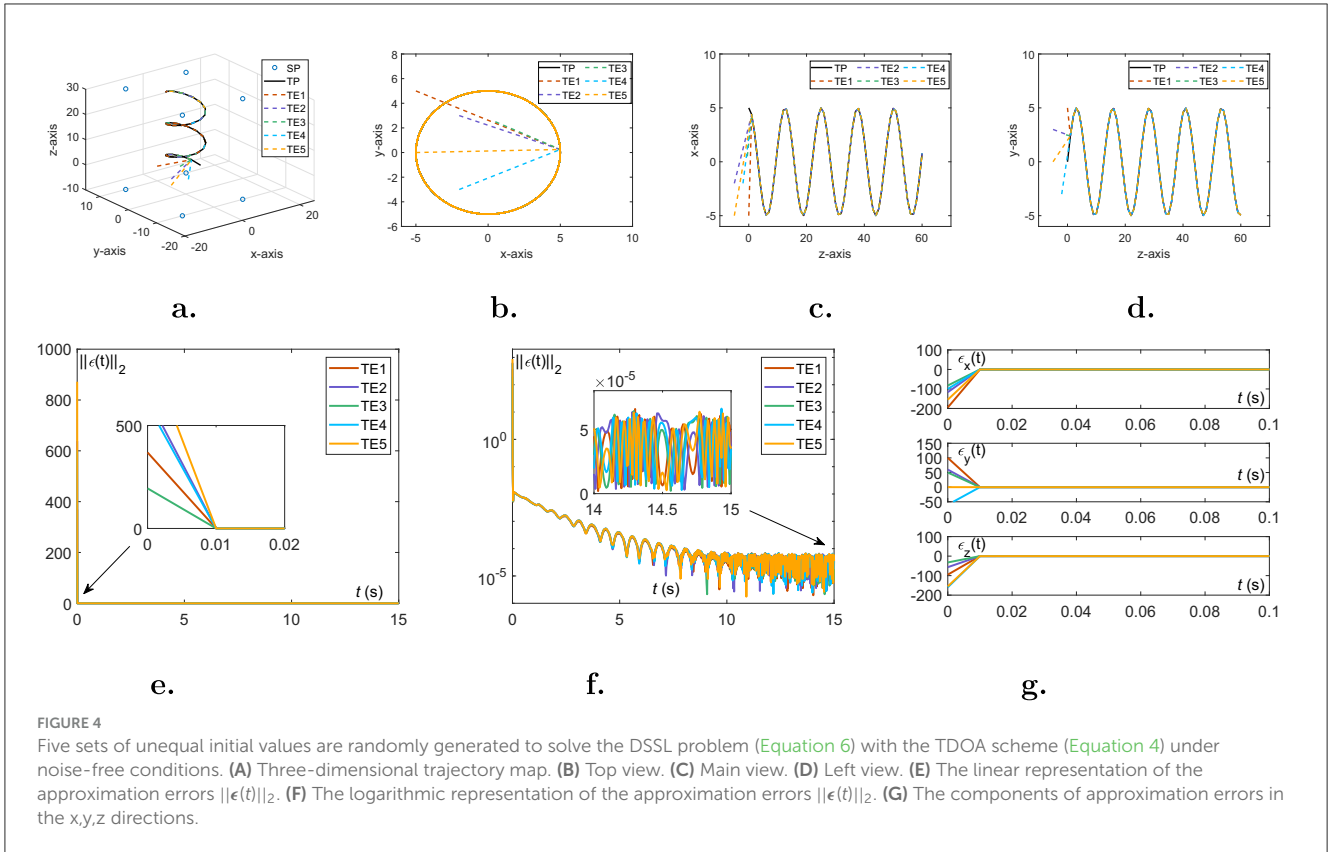


FIGURE 4

Five sets of unequal initial values are randomly generated to solve the DSSL problem (Equation 6) with the TDOA scheme (Equation 4) under noise-free conditions. (A) Three-dimensional trajectory map. (B) Top view. (C) Main view. (D) Left view. (E) The linear representation of the approximation errors $\|\epsilon(t)\|_2$. (F) The logarithmic representation of the approximation errors $\|\epsilon(t)\|_2$. (G) The components of approximation errors in the x,y,z directions.

TABLE 2 Comparison of the average steady-state residual error (ASSRE) and maximum steady-state residual error (MSSRE) among TGND model, TZND model, and the proposed NIZND model (Equation 13) when solving the DSSL problem (Equation 6) using the TDOA scheme (Equation 4).

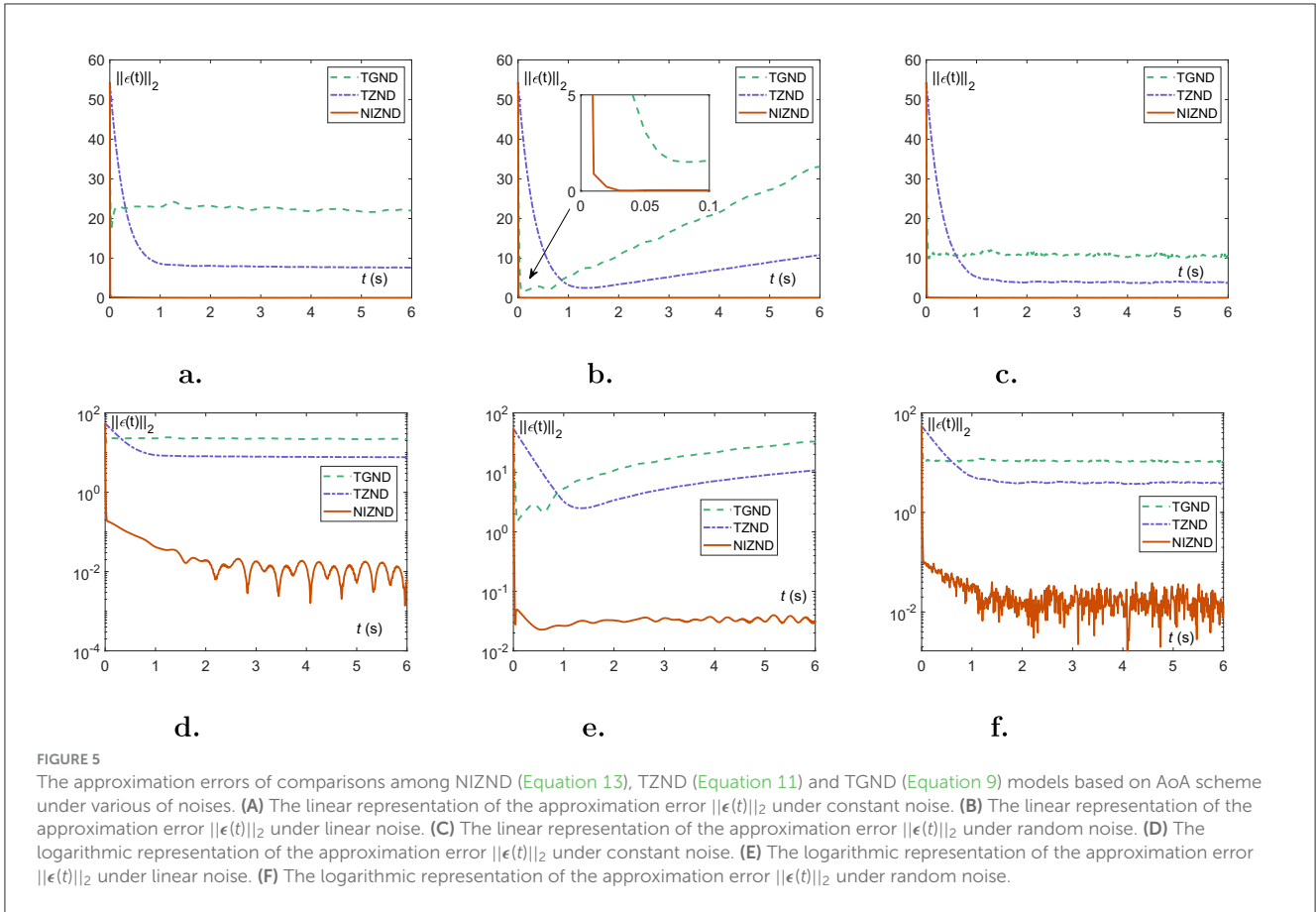
Model	Parameters	Average steady-state residual error				Maximal steady-state residual error			
		with NF*	with CN*	with LN*	with RN*	with NF*	with CN*	with LN*	with RN*
TGND	$\omega = 3$	6.404×10^0	2.019×10^1	Infinity	1.043×10^1	1.037×10^1	2.225×10^1	Infinity	1.541×10^1
	$\omega = 20$	6.193×10^{-1}	2.017×10^1	Infinity	1.018×10^1	2.024×10^0	2.182×10^1	Infinity	1.483×10^1
TZND	$\kappa = 3$	4.726×10^{-2}	6.418×10^0	Infinity	3.333×10^0	1.174×10^{-1}	6.719×10^0	Infinity	3.849×10^0
	$\kappa = 20$	2.246×10^{-2}	1.006×10^0	Infinity	5.221×10^{-1}	6.632×10^{-2}	1.101×10^0	Infinity	7.771×10^{-1}
NIZND	$\gamma = 3, \mu = 3$	3.917×10^{-5}	5.636×10^{-3}	2.780×10^{-2}	1.752×10^{-2}	7.236×10^{-5}	1.951×10^{-2}	3.350×10^{-2}	3.506×10^{-2}
	$\gamma = 20, \mu = 20$	3.895×10^{-4}	4.241×10^{-4}	7.759×10^{-4}	2.607×10^{-3}	7.207×10^{-4}	8.047×10^{-4}	1.557×10^{-3}	7.007×10^{-3}

*NF, CN, LN, and RN indicate noise free, constant noise 8, linear noise 2t, and random noise $8 \times [0, 1]$, respectively.

TZND models (Equation 11) are of divergence. As Table 1 depicted, the average steady-state residual error and maximum steady-state residual error of the TGND (Equation 9) and TZND (Equation 11) models converge to infinity. Considering the case of linear noises in Figures 5C, F, we can see that the error of the proposed NIZND model (13) resulted in the lowest value of the number. Specifically, Table 1 also shows the same results.

Likewise, the experimental results for the TDOA scheme 4 have a similar trend to the experimental results for the AoA scheme (Equations 1, 2). It is worth mentioning that Figures 6B, E and Table 2 can demonstrate the convergence of the TGND model (Equation 9) and the TZND model (Equation 11) for solving

the DSSL problem (Equation 6), which is undoubtedly a great challenge for dynamic localization from the real environment. Under noises situation, combing with the visualization results (Equation 6), both the (Equation 9) and the TZND model (Equation 11) are worse than that of the proposed NIZND model (Equation 13). Of the Table 2, the average steady-state residual error and maximum steady-state residual error of the proposed NIZND model (Equation 13) are also less than those of the other two comparison models. Furthermore, the larger the coefficients γ, μ of the proposed NIZND model (Equation 13), the higher its convergence accuracy under noisy conditions, which indicates the strong robustness of the proposed model (Equation 13).



5.4 Application to the robotic manipulator

To further demonstrate the effectiveness and robustness of the proposed NIZND model (Equation 13), a simulation is conducted on a robotic manipulator employing NIZND model (Equation 13) for achieving precise trajectory tracking. The trajectory tracking of a robotic manipulator is to obtain the joint angle $\theta(t)$ for the desired trajectory $r_d(t)$ at each time instant. Specifically, the trajectory tracking of a robotic manipulator is achieved by solving the following equation:

$$J(\theta(t))\dot{\theta}(t) = \dot{r}_d(t), \tag{30}$$

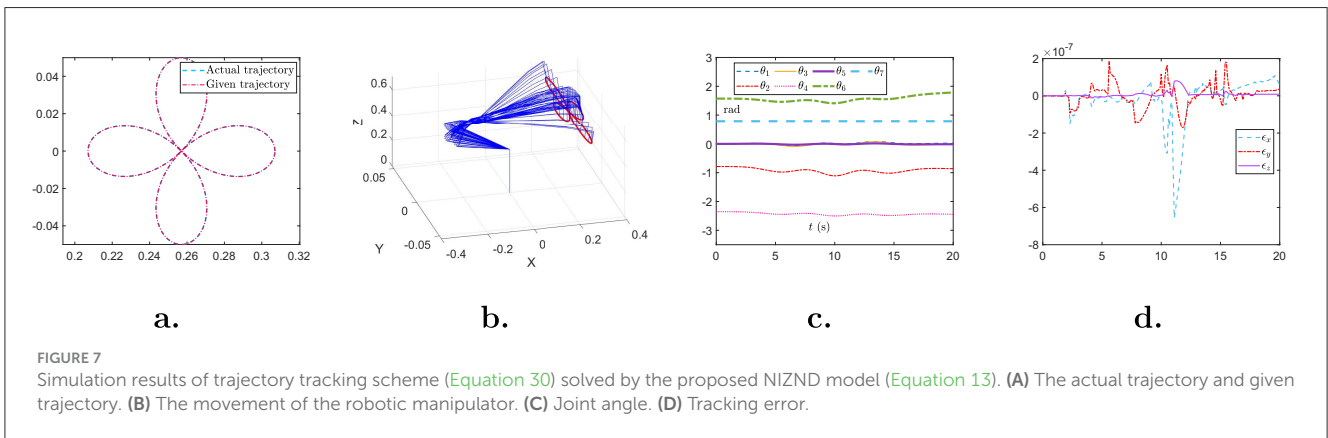
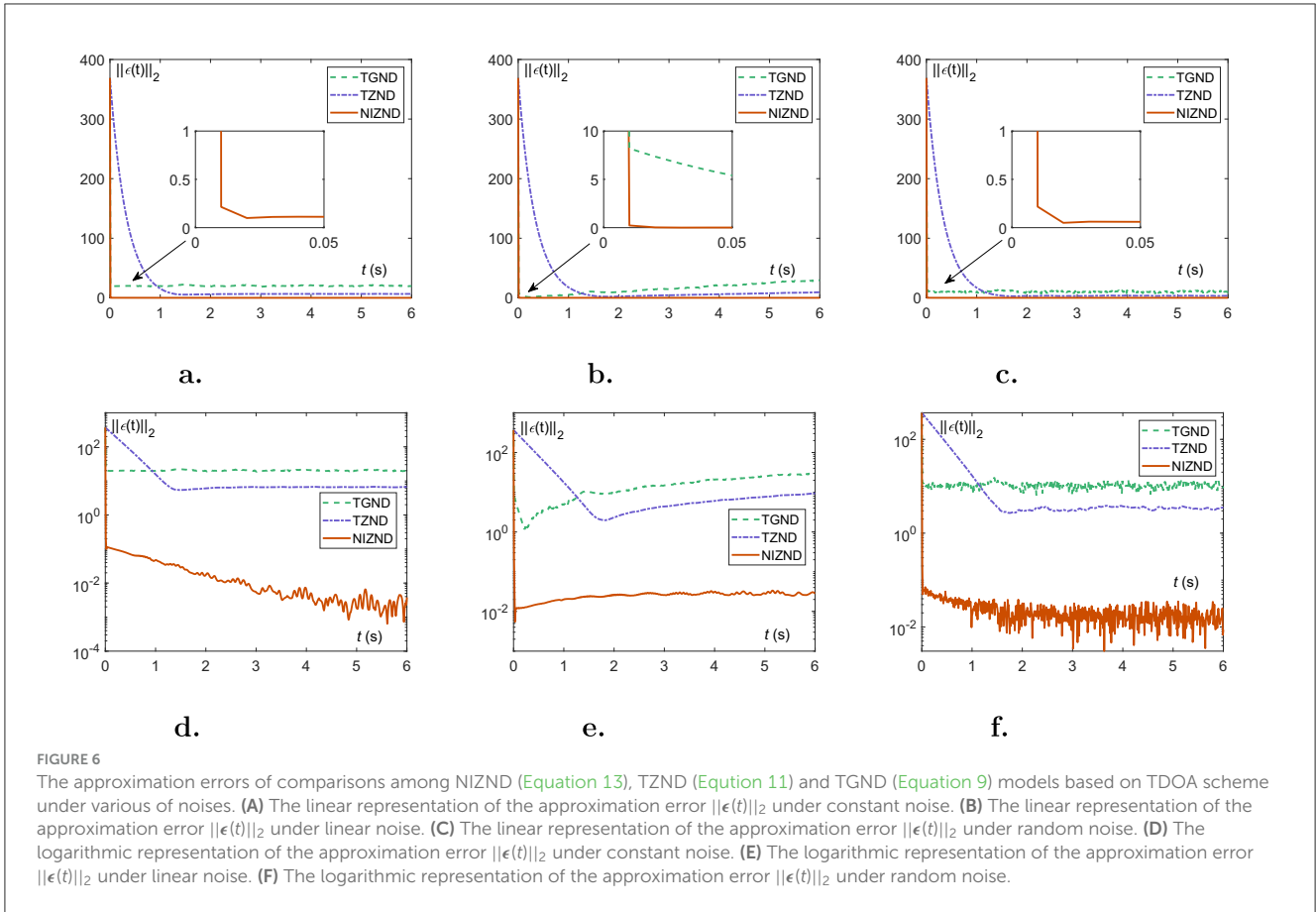
where $J(\theta(t))$ represents the Jacobian matrix and $\dot{\theta}(t)$ is the joint velocity. Then, the proposed NIZND model (Equation 13) is employed to obtain the solution to trajectory tracking scheme (Equation 30) under noise perturbation. Simulation results are shown in Figure 7. Figure 7A depicts the actual trajectory and given trajectory of the robotic manipulator. The movement process is displayed in Figure 7B. Figures 7C, D illustrate the joint angle and tracking error during the tracking task. Solved by NIZND model (Equation 13), the trajectory tracking task is successfully accomplished with minor tracking error, demonstrating the effectiveness and robustness of the proposed NIZND model (Equation 13).

5.5 Summary

In summary, the proposed NIZND model (Equation 13) demonstrates superiority over the three models. Moreover, these comparative results suggest an association between convergence performance and the coefficients taken. In the above experiments, by comparing the performance differences between the models under the same noise conditions, it is clear that the proposed NIZND model (Equation 13) is characterized by high convergence accuracy and strong robustness. In general, the proposed NIZND model (Equation 13) has a higher convergence accuracy in the noise-free condition. In addition, its strong robustness enables it to maintain good convergence performance under the three noise conditions. In contrast, the robustness is enhanced by increasing the values of the two coefficients of the proposed NIZND model (Equation 13), which can be adapted to complicated noise disturbances in realistic environments.

6 Conclusion

In this paper, a novel noise-immune zeroing neural dynamics (NIZND) model has been proposed for solving the dynamic signal source localization tracking (DSSL) and robotic trajectory tracking problem. Additionally, taking into account the effect of noise in



real scenes, four theorems, and the corresponding proof process are presented. Specifically, the results of the proposed theorems are shown that the proposed NIZND model process global convergence and enhances robustness. Then, the superiority of the model in solving the DSSL problem was verified by computer simulations and experiments compared to other models. Additionally, it has been applied in a robotic manipulator to further demonstrate the effectiveness and robustness of the proposed NIZND model. Finally, it is worth mentioning that possible future investigations will optimize the proposed NIZND model to better cope with the problems posed by realistic DSSL.

Data availability statement

The original contributions presented in the study are included in the article/supplementary material, further inquiries can be directed to the corresponding author.

Author contributions

YZ: Conceptualization, Methodology, Writing – original draft. JW: Investigation, Methodology, Project administration,

Writing – review & editing. MZ: Writing – review & editing.

Funding

The author(s) declare that no financial support was received for the research, authorship, and/or publication of this article.

Conflict of interest

The authors declare that the research was conducted in the absence of any commercial or financial relationships that could be construed as a potential conflict of interest.

References

- Ali, W. H., Kareem, A. A., and Jasim, M. (2019). Survey on wireless indoor positioning systems. *Cihan Univ. Erbil Sci. J.* 3, 42–47. doi: 10.24086/cuesj.v3n2y2019.pp42-47
- Dai, J., Li, Y., Xiao, L., and Jia, L. (2021). Zeroing neural network for time-varying linear equations with application to dynamic positioning. *IEEE Trans. Ind. Inform.* 18, 1552–1561. doi: 10.1109/TII.2021.3087202
- Dai, L., Xu, H., Zhang, Y., and Liao, B. (2024). Norm-based zeroing neural dynamics for time-variant non-linear equations. *CAAI Trans. Intell. Technol.* 14, 1561–1571. doi: 10.1049/cit2.12360
- Ferreira, L. V., Kaszkurewicz, E., and Bhaya, A. (2005). Solving systems of linear equations via gradient systems with discontinuous righthand sides: application to LS-SVM. *IEEE Trans. Neural Netw.* 16, 501–505. doi: 10.1109/TNN.2005.844091
- Guo, X., Ansari, N., Hu, F., Shao, Y., Elikplim, N. R., and Li, L. (2019a). A survey on fusion-based indoor positioning. *IEEE Commun. Surv. Tutor.* 22, 566–594. doi: 10.1109/COMST.2019.2951036
- Guo, X., Chen, Z., Hu, X., and Li, X. (2019b). Multi-source localization using time of arrival self-clustering method in wireless sensor networks. *IEEE Access* 7, 82110–82121. doi: 10.1109/ACCESS.2019.2923771
- Hong, C.-Y., Wu, Y.-C., Liu, Y., Chow, C.-W., Yeh, C.-H., Hsu, K.-L., et al. (2020). Angle-of-arrival (AOA) visible light positioning (VLP) system using solar cells with third-order regression and ridge regression algorithms. *IEEE Photonics J.* 12, 1–5. doi: 10.1109/JPHOT.2020.2993031
- Jiang, M. and Wang, G. (2003). Convergence studies on iterative algorithms for image reconstruction. *IEEE Trans. Med. Imag.* 22, 569–579. doi: 10.1109/TMI.2003.812253
- Jin, L., Chen, Y., and Liu, M. (2024a). A noise-tolerant k -wta model with its application on multirobot system. *IEEE Trans. Ind. Inform.* 20, 3574–3584. doi: 10.1109/TII.2023.3308330
- Jin, L., Huang, R., Liu, M., and Ma, X. (2024b). Cerebellum-inspired learning and control scheme for redundant manipulators at joint velocity level. *IEEE Trans. Cybern.* 54, 6297–6306. doi: 10.1109/TCYB.2024.3436021
- Jin, L., Wei, L., and Li, S. (2022). Gradient-based differential neural-solution to time-dependent nonlinear optimization. *IEEE Trans. Automat. Contr.* 68, 620–627. doi: 10.1109/TAC.2022.3144135
- Jin, L., Yan, J., Du, X., Xiao, X., and Fu, D. (2020). Rnn for solving time-variant generalized Sylvester equation with applications to robots and acoustic source localization. *IEEE Trans. Ind. Inform.* 16, 6359–6369. doi: 10.1109/TII.2020.2964817
- Jin, L., Zhang, Y., Li, S., and Zhang, Y. (2016). Modified znn for time-varying quadratic programming with inherent tolerance to noises and its application to kinematic redundancy resolution of robot manipulators. *IEEE Trans. Industr. Electr.* 63, 6978–6988. doi: 10.1109/TIE.2016.2590379
- Jin, L., Zhao, J., Chen, L., and Li, S. (2024c). Collective neural dynamics for sparse motion planning of redundant manipulators without hessian matrix inversion. *IEEE Trans. Neural Netw. Learn. Syst.* 11, 1–24. doi: 10.1109/TNNLS.2024.3363241
- Kunhoth, J., Karkar, A., Al-Maadeed, S., and Al-Ali, A. (2020). Indoor positioning and wayfinding systems: a survey. *Hum. Centr. Comput. Inf. Sci.* 10, 1–41. doi: 10.1186/s13673-020-00222-0
- Li, W., Liao, B., Xiao, L., and Lu, R. (2019a). A recurrent neural network with predefined-time convergence and improved noise tolerance for dynamic matrix

Generative AI statement

The author(s) declare that no Gen AI was used in the creation of this manuscript.

Publisher's note

All claims expressed in this article are solely those of the authors and do not necessarily represent those of their affiliated organizations, or those of the publisher, the editors and the reviewers. Any product that may be evaluated in this article, or claim that may be made by its manufacturer, is not guaranteed or endorsed by the publisher.

square root finding. *Neurocomputing* 337, 262–273. doi: 10.1016/j.neucom.2019.01.072

Li, W., Xiao, L., and Liao, B. (2019b). A finite-time convergent and noise-rejection recurrent neural network and its discretization for dynamic nonlinear equations solving. *IEEE Trans. Cybern.* 50, 3195–3207. doi: 10.1109/TCYB.2019.2906263

Lian, Y., Xiao, X., Zhang, J., Jin, L., Yu, J., and Sun, Z. (2024). Neural dynamics for cooperative motion control of omnidirectional mobile manipulators in the presence of noises: a distributed approach. *IEEE/CAA J. Autom. Sinica* 11, 1605–1620. doi: 10.1109/JAS.2024.124425

Liao, B., Han, L., Cao, X., Li, S., and Li, J. (2024). Double integral-enhanced zeroing neural network with linear noise rejection for time-varying matrix inverse. *CAAI Trans. Intell. Technol.* 9, 197–210. doi: 10.1049/cit2.12161

Liao, B., Wang, Y., Li, J., Guo, D., and He, Y. (2022). Harmonic noise-tolerant znn for dynamic matrix pseudoinversion and its application to robot manipulator. *Front. Neurobot.* 16:928636. doi: 10.3389/fnbot.2022.928636

Liu, M., Li, Y., Chen, Y., Qi, Y., and Jin, L. (2024). A distributed competitive and collaborative coordination for multirobot systems. *IEEE Trans. Mobile Comput.* 23, 11436–11448. doi: 10.1109/TMC.2024.3397242

Liu, M., Zhang, X., Shang, M., and Jin, L. (2022). Gradient-based differential k WTA network with application to competitive coordination of multiple robots. *IEEE/CAA J. Autom. Sinica* 9, 1452–1463. doi: 10.1109/JAS.2022.105731

Lv, X., Xiao, L., Tan, Z., Yang, Z., and Yuan, J. (2019). Improved gradient neural networks for solving moore-penrose inverse of full-rank matrix. *Neural Proc. Lett.* 50, 1993–2005. doi: 10.1007/s11063-019-09983-x

Monfared, S., Copa, E. I. P., De Doncker, P., and Horlin, F. (2021). Aoa-based iterative positioning of iot sensors with anchor selection in nlos environments. *IEEE Trans. Vehic. Technol.* 70, 6211–6216. doi: 10.1109/TVT.2021.3077462

Monfared, S., Nguyen, T.-H., Van der Vorst, T., De Doncker, P., and Horlin, F. (2020). Iterative nda positioning using angle-of-arrival measurements for IoT sensor networks. *IEEE Trans. Vehic. Technol.* 69, 11369–11382. doi: 10.1109/TVT.2020.3009760

Nassar, M. A., Luxford, L., Cole, P., Oatley, G., and Koutsakis, P. (2019). The current and future role of smart street furniture in smart cities. *IEEE Commun. Magaz.* 57, 68–73. doi: 10.1109/MCOM.2019.1800979

Pérez-Solano, J. J., Ezpeleta, S., and Claver, J. M. (2020). Indoor localization using time difference of arrival with UWB signals and unsynchronized devices. *Ad Hoc Netw.* 99:102067. doi: 10.1016/j.adhoc.2019.102067

Sun, Z., Tang, S., Fei, Y., Xiao, X., Hu, Y., and Yu, J. (2024). An orthogonal repetitive motion and obstacle avoidance scheme for omnidirectional mobile robotic arm. *IEEE Trans. Ind. Electr.* doi: 10.1109/TIE.2024.3451063

Sun, Z., Tang, S., Jin, L., Zhang, J., and Yu, J. (2003). Nonconvex activation noise-suppressing neural network for time-varying quadratic programming: application to omnidirectional mobile manipulator. *IEEE Trans. Ind. Inform.* 19, 10786–10798. doi: 10.1109/TII.2023.3241683

Sun, Z., Wang, G., Jin, L., Cheng, C., Zhang, B., and Yu, J. (2022). Noise-suppressing zeroing neural network for online solving time-varying matrix square roots problems: a control-theoretic approach. *Expert Syst. Appl.* 192:116272. doi: 10.1016/j.eswa.2021.116272

- Tang, Z. and Zhang, Y. (2023). Continuous and discrete gradient-zhang neuronet (GZN) with analyses for time-variant overdetermined linear equation system solving as well as mobile localization applications. *Neurocomputing* 561:126883. doi: 10.1016/j.neucom.2023.126883
- Wang, X., Huang, G., Benesty, J., Chen, J., and Cohen, I. (2020). Time difference of arrival estimation based on a kronecker product decomposition. *IEEE Signal Process. Lett.* 28, 51–55. doi: 10.1109/LSP.2020.3044775
- Wu, D., Li, Z., Yu, Z., He, Y., and Luo, X. (2023). Robust low-rank latent feature analysis for spatiotemporal signal recovery. *IEEE Trans. Neural Netw. Learn. Syst.* 99, 1–14. doi: 10.1109/TNNLS.2023.3339786
- Wu, P., Su, S., Zuo, Z., Guo, X., Sun, B., and Wen, X. (2019). Time difference of arrival (TDOA) localization combining weighted least squares and firefly algorithm. *Sensors* 19:2554. doi: 10.3390/s19112554
- Wu, S., Zhang, S., and Huang, D. (2019a). A TOA-based localization algorithm with simultaneous nlos mitigation and synchronization error elimination. *IEEE Sensors Lett.* 3, 1–4. doi: 10.1109/LENS.2019.2897924
- Wu, S., Zhang, S., Xu, K., and Huang, D. (2019b). Neural network localization with TOA measurements based on error learning and matching. *IEEE Access* 7, 19089–19099. doi: 10.1109/ACCESS.2019.2897153
- Xiao, L., Zhang, Y., Li, K., Liao, B., and Tan, Z. (2019). A novel recurrent neural network and its finite-time solution to time-varying complex matrix inversion. *Neurocomputing* 331, 483–492. doi: 10.1016/j.neucom.2018.11.071
- Xiao, X., Fu, D., Wang, G., Liao, S., Qi, Y., Huang, H., et al. (2020). Two neural dynamics approaches for computing system of time-varying nonlinear equations. *Neurocomputing* 394, 84–94. doi: 10.1016/j.neucom.2020.02.011
- Xie, Z. and Jin, L. (2023). A fuzzy neural controller for model-free control of redundant manipulators with unknown kinematic parameters. *IEEE Trans. Fuzzy Syst.* 32, 1589–1601. doi: 10.1109/TFUZZ.2023.3328545
- Xie, Z., Jin, L., and Lv, X. (2024a). A hierarchical control and learning network for redundant manipulators with unknown physical parameters. *IEEE Trans. Ind. Electr.* 2024, 1–19. doi: 10.1109/TIE.2024.3497304
- Xie, Z., Liu, M., Su, Z., Sun, Z., and Jin, L. (2024b). A data-driven obstacle avoidance scheme for redundant robots with unknown structures. *IEEE Trans. Ind. Inform.* 34, 1–10. doi: 10.1109/TII.2024.3488775
- Xu, S., Ou, Y., Wang, Z., Duan, J., and Li, H. (2020). Learning-based kinematic control using position and velocity errors for robot trajectory tracking. *IEEE Trans. Syst. Man Cybern. Syst.* 52, 1100–1110. doi: 10.1109/TSMC.2020.3013904
- Yan, J., Jin, L., Yuan, Z., and Liu, Z. (2021). Rnn for receding horizon control of redundant robot manipulators. *IEEE Trans. Ind. Electr.* 69, 1608–1619. doi: 10.1109/TIE.2021.3062257
- Yang, H., Li, D., Xu, X., and Zhang, H. (2022). An obstacle avoidance and trajectory tracking algorithm for redundant manipulator end. *IEEE Access* 10, 52912–52921. doi: 10.1109/ACCESS.2022.3173404
- Zare, M., Battulwar, R., Seamons, J., and Sattarvand, J. (2021). Applications of wireless indoor positioning systems and technologies in underground mining: a review. *Mining, Metal. Explor.* 38, 2307–2322. doi: 10.1007/s42461-021-00476-x
- Zhai, J. and Xu, G. (2020). A novel non-singular terminal sliding mode trajectory tracking control for robotic manipulators. *IEEE Trans. Circ. Syst.* 68, 391–395. doi: 10.1109/TCSII.2020.2999937
- Zhang, Y., Li, S., Kadry, S., and Liao, B. (2018). Recurrent neural network for kinematic control of redundant manipulators with periodic input disturbance and physical constraints. *IEEE Trans. Cybern.* 49, 4194–4205. doi: 10.1109/TCYB.2018.2859751
- Zhang, Y., Li, S., Weng, J., and Liao, B. (2024). Gnn model for time-varying matrix inversion with robust finite-time convergence. *IEEE Trans. Neural Netw. Learn. Syst.* 35, 559–569. doi: 10.1109/TNNLS.2022.3175899
- Zhao, W., Panerati, J., and Schoellig, A. P. (2021). Learning-based bias correction for time difference of arrival ultra-wideband localization of resource-constrained mobile robots. *IEEE Robot. Autom. Lett.* 6, 3639–3646. doi: 10.1109/LRA.2021.3064199
- Zhou, T., Xu, K., Shen, Z., Xie, W., Zhang, D., and Xu, J. (2022). Aoa-based positioning for aerial intelligent reflecting surface-aided wireless communications: an angle-domain approach. *IEEE Wirel. Commun. Lett.* 11, 761–765. doi: 10.1109/LWC.2022.3143099